Bull Earthquake Eng (2018) 16:155–182
https://doi.org/10.1007/s10518-017-0197-4

ORIGINAL RESEARCH PAPER

Convex model-based calculation of robust seismic fragility curves of isolated continuous girder bridge

X. H. Long[1,2] · Z. Y. Xie[1] · J. Fan[1,2] · Y. Miao[1]

Received: 8 December 2016 / Accepted: 17 July 2017 / Published online: 24 July 2017

Abstract The convex model approach is applied to derive the robust seismic fragility curves of a five-span isolated continuous girder bridge with lead rubber bearings (LRB) in China. The uncertainty of structure parameters (the yield force and the post-yield stiffness of LRB, the yield strength of steel bars, etc.) are considered in the convex model, and the uncertainty of earthquake ground motions is also taken into account by selecting 40 earthquake excitations of peak ground acceleration magnitudes ranging from 0.125 to 1.126 g. A 3-D finite element model is employed using the software package OpenSees by considering the nonlinearity in the bridge piers and the isolation bearings. Section ductility of piers and shearing strain isolation bearings are treated as damage indices. The cloud method and convex model approach are used to construct the seismic fragility curves of the bridge components (LRB and bridge piers) and the bridge system, respectively. The numerical results indicate that seismic fragility of the bridge system and bridge components will be underestimated without considering the uncertainty of structural parameters. Therefore, the failure probability $P_{f,max}$ had better be served as the seismic fragility, especially, the fragility of the bridge system is largely dictated by the fragility of LRB. Finally, the probabilistic seismic performance evaluation of the bridge is carried out according to the structural seismic risk estimate method.

Keywords Convex model · Isolated continuous girder bridge · Lead rubber bearing · Seismic fragility · Could method · Response surface method

✉ X. H. Long
xhlong@hust.edu.cn

[1] School of Civil Engineering and Mechanics, Huazhong University of Science and Technology, Wuhan, Hubei 430074, People's Republic of China

[2] Hubei Key Laboratory of Control Structure, Huazhong University of Science and Technology, Wuhan, Hubei 430074, People's Republic of China

1 Introduction

Since pacific earthquake engineering research (PEER) put forward the theoretical framework of the next generation performance-based earthquake engineering (PBEE), structure seismic fragility analysis have gained more concern as an important component of the PBEE (FEMA 2006; Padgett et al. 2008). Seismic fragility analysis evaluates the probability of a certain damage state when structures are subjected to different earthquake magnitudes. The analysis methods of seismic fragility commonly include empirical, statistical and numerical analysis (Shinozuka et al. 2000a, b; Karim and Yamazaki 2001a, b; Hwang et al. 2001; Moschonas et al. 2009; Billah and Alam 2015). Although, the seismic isolation technique has been widely used in bridge engineering, the destruction data of isolated bridges subjected to earthquakes is still rare. Thus, the numerical analysis method is the only effective way to derive the seismic fragility of isolated bridges. Currently, probability model is usually employed in the seismic fragility analysis of the bridge structures, the characteristics of the model is that probability density function of random variables must be defined in advance. Nevertheless, the probability density functions of mechanical parameters (e.g. yield force and post-yield stiffness) of lead rubber bearings (LRB) are unknown and rarely reported in present papers. Therefore, how to accurately take into account uncertainties of lead rubber bearings will be a significant factor of seismic fragility analysis of isolated bridges.

The probabilistic seismic demand model (PSDM), which represents the statistical relationship between intensity measure (IM) and engineering demand parameters (EDPs), is commonly considered as the base of seismic fragility analysis. Traditional probabilistic seismic demand analysis (PSDA) was proposed by Shome (1999) for the first time, then Cornell and Krawinkler (2000) improved the theoretical system of this method in order to enhance its practicability. Generally, there are two kinds of calculation methods for seismic demand: one is parametric analysis method which assumes that earthquake demand parameters obey definite probability distribution (such as normal distribution or exponential normal distribution). Moreover, probability distribution functions of EDPs can be confirmed by estimating a little amount of model parameters (e.g. mean value adn variance value), and then the probabilistic seismic demand model could be established. Karim and Yamazaki (2007) employed the simplified fragility analysis method to derive the fragility curves of piers of isolated bridges, and the result showed that LRBs could effectively reduce the possible damage of bridge piers. Zhang and Huo (2009) studied the optimal design of isolated bearings of isolated bridges using seismic fragility method. The second method is called non-parametric analysis that the empirical probability of probabilistic seismic demand models can be directly calculated under different earthquake ground motion intensity measures. However, distribution types of EDPs may be not assumed in this method.

Probabilistic model method needs a great amount of sample data that is very hard to receive in practical engineering, while non-probabilistic convex model approach can be established with less information. Although probability distribution functions remain unknown, the boundaries of uncertainty parameters can be determined according to the available information and be described with the convex set (such as interval set or ellipsoid set), so that the non-probabilistic set-theory can be introduced into engineering to solve all kinds of uncertain problems (Qiu and Wang 2010). The description method on the uncertain set first appeared in the 1960s. Elishakoff (1995) compared stochastic model and non-stochastic model with convex model to illustrate the defections of probabilistic method, which need enough accurate data and the significant result errors induced by input errors. Moreover, he also put forward the non-probabilistic convex model for the unknown

probabilistic distribution of design parameters. Pantelides and Tzan (1996) illustrated that the responses obtained by the convex model were relatively larger than the results calculated by the normal way, so they developed a reduction factor to adjust the results obtained by the convex model. Fan et al. (2014) considered uncertainties of isolated structure parameters with the convex model and proposed a new calculation method for collision fragility curves of base isolated building subjected to near-fault earthquake excitation, and uncertainties of structures and earthquake ground motion were simultaneously taken into account.

For the seismic response analysis of structures, two methods may be employed by considering structural uncertainty factors: probabilistic model based on the mathematical statistics and non-probabilistic convex model based on the convex theory. The design mechanical parameters (e.g. yield force, post-yield stiffness) of the isolated bridge are very sensitive to isolation effect on the structure. Though the probabilistic distribution functions of LRBs are rarely mentioned in the recent research, national standard for rubber bearings provides the bound values of these parameters (such as allowable deviation of shearing property of bearings type S–A is within ±10%, and that of shearing property of bearings type S–B is within ±20%) (GB/T 20688.1-2007 2007). In order to better describe the uncertainties of structure parameters, the convex model is introduced into seismic fragility analysis of isolated bridge in this paper. The objective of the work is to access the vulnerability and seismic performance of a isolated continuous girder bridge with Lead rubber bearings (LRB) when subjected to a total of 40 earthquake excitations of peak ground acceleration (PGA) magnitudes ranging from 0.125 to 1.126 g. The cloud method and convex model approach are used to evaluate the seismic fragility, respectively, which is based on the results obtained from the nonlinear time-history analysis using software package OpenSees (McKenna and Fenves 2001). A 3-D finite element model with the nonlinear beam-column element for bridge piers and and zero length bilinear link element for LRBs is built. The response functions in variable space of bridge components can be obtained by the response surface method, and the maximum and minimum values of response surfaces can be calculated by the optimization function in MATLAB. Thus, robust fragility curves of bridge components and the bridge system bridge piers and LRBs can be constructed. Finally, the probabilistic seismic performance evaluation of the bridge is carried out according to the structural seismic risk estimate method.

2 Convex model approach

Here is the definition of convex set: Let $S \in E^N$, if random points P and Q belong to S ($P \in S, Q \in S$), and the point $\alpha P + (1 - \alpha)Q$ also belongs to S, in which $0 \leq \alpha \leq 1$, then we call S a convex set. According to this definition, we can know that the convex set has the following characteristic: if two points belong to one convex set, the line segment between two points must belong to the convex set, this property which can be applied to the fitting of response surface. There are several convex models which can be selected by considering features of uncertain variables. And the simpler model is the maximum bound convex model (MB), which has been widely used for the simple form and few information. The MB model is defined as follow: absolute value of each component of uncertain variables is under a limit, which can be expressed as

$$\Omega_{MB} = \left\{\alpha(t) \in R^r : \left|\alpha_j(t) \leq \overline{\alpha}_j, \quad j = 1, \ldots, r\right\}\right. \tag{1}$$

where $\bar{\alpha}_j$ are constant.

Let $X = [X_1, X_2, \ldots, X_n]$ is the convex vector that represents uncertainties of structure material, and the uncertain variable I is described as uncertainty of earthquake ground motions. So, the structural seismic response can be expressed as $S(X, I)$, where $x_i \in X_i$, x_i can be written as

$$x_i = (1 + \gamma_i \delta_i) x_i^c \tag{2}$$

where $x_i^c = (x_i^l + x_i^u)/2$ is the mean value of x_i, γ_i is the deviation rate of x_i, x_i^l, x_i^u are the upper and lower bounds of x_i, respectively, and standardized variable $\delta_i \in [-1, 1]$. In consideration of the related restriction or mutual independence among uncertain parameters, which would be grouped according to the correlation. Three parameters are selected as uncertain variables, namely yield force of LRBs δ_1, the post-yield stiffness of LRBs δ_2, the yield strength of steel bars δ_3. Therefore, the standard variable can be expressed as $\boldsymbol{\delta} = [\{\delta_1, \delta_2\}, \delta_3]$. If we define δ_i with multi-unit super-sphere set, standard variables can be defined as

$$\boldsymbol{\delta} \in E = \{\boldsymbol{\delta} : \delta_i \delta_i^T \leq 1, \quad i = 1, 2, \ldots, m\} \tag{3}$$

where δ_1 and δ_2 are combined as one group by considering of the correction. E is a multi-unit super-sphere set containing two groups of uncertain parameters. Since E represents a convex set, the uncertain parameters model expressed as Eq. (3) is defined as the convex model.

N earthquake ground motions are selected by latin hypercube sampling (LHS), and the ith of them is chosen as seismic input to conduct nonlinear time history analysis in order to obtain the maximum responses of LRBs and bridge piers, which can be assumed as $S(\boldsymbol{\delta}, I = i)$. Since $\boldsymbol{\delta}$ belongs to the convex domain described by Eq. (4), $S(\boldsymbol{\delta}, I = i)$ also have boundaries as shown below

$$\begin{aligned} S_{\max}(I = i) &= \sup_{\delta \in E} \{S(\boldsymbol{\delta}, I = i)\}, \\ S_{\min}(I = i) &= \inf_{\delta \in E} \{S(\boldsymbol{\delta}, I = i)\}. \end{aligned} \tag{4}$$

The boundaries can be obtained by solving constrained optimization problems.

$$\begin{aligned} &find\ \delta \\ &S_{\min}(I = i) = \min(S(\boldsymbol{\delta}, I = i)) \\ &S_{\max}(I = i) = \max(S(\boldsymbol{\delta}, I = i)) \\ &s.t. \quad \delta_i \cdot \delta_i^T \leq 1, \quad i = 1, 2, \ldots, m \end{aligned} \tag{5}$$

where $S(\boldsymbol{\delta}, I = i)$ is not an explicit expression. Obviously, this implicit function needs to be transformed into explicit expression just to gain its extreme value. Quadratic polynomial response surface method is applied in this paper to acquire the explicit expression $\overline{S}(\boldsymbol{\delta}, I = i)$, Subsequently, the maximum value $S_{\max}(I = i)$ and the minimum value $S_{\min}(I = i)$ of this expression can be solved.

3 Methodology of fragility analysis and seismic performance evaluation

3.1 Cloud method

Probabilistic seismic demand model (PSDM) is used to derive analytical fragility functions. PSDM is to establish a statistical relationship between engineering demand parameters (EDP) and the ground motion Intensity Measure (IM). The PSDA method utilizes regression analysis to obtain the mean and standard deviation for each limit state by assuming the logarithmic correlation between the median EDP and the selected IM.

$$\ln(EDP) = \ln a + b\ln(IM) \tag{6}$$

where the parameters a and b are regression coefficients obtained from the nonlinear time-history response analysis. The standard deviation can be estimated as

$$\xi_{EDP/IM} = \sqrt{\frac{\sum_{i=1}^{n}\left[\ln(EDP_i) - (\ln a + b\ln IM_i)\right]^2}{n-2}} \tag{7}$$

seismic fragility functions of the bridge structure describe the conditional probability of reaching a certain limit state (LS) under different seismic IM. The failure probability of the certain LS can be expressed as (Alam et al. 2012)

$$P_f = P(DI \geq LS/IM) = \Phi\left(\frac{\ln(aIM^b) - \ln(LS)}{\xi_{EDP/IM}}\right) \tag{8}$$

where $\xi_{EDP/IM}$ is the standard deviation of the logarithmic distribution that computed from Eq. (7), and $\Phi(\cdot)$ is the standard normal distribution function.

Different definitions exist among the engineering field in different countries for the definition of the structural damage state in the seismic fragility analysis. The common damage indices for bridge structures are shown in Table 1. Based on the results of numerous studies, the ductility of a pier section μ_κ is selected as the pier damage index and

Table 1 Damage indices of piers and isolation bearings under different limit states

Bridge component	Damage index	Slight (LS1)	Moderate (LS2)	Extensive (LS3)	Collapsed (LS4)
Bridge pier	A. Section ductility μ_κ	$\mu_\kappa > 1$	$\mu_\kappa > 2$	$\mu_\kappa > 4$	$\mu_\kappa > 7$
	B. Displacement ductility μ_d	$\mu_d > \mu_{first-yield}$ (1.0)	$\mu_d > \mu_{yield}$ (1.20)	$\mu_d > \mu_{\varepsilon c=0.002}$ (1.76)	$\mu_d > \mu_{\max}$ (4.76)
	C. $\eta = (\mu_d + \beta\mu_h)/\mu_u$	$\eta > 0.14$	$\eta > 0.40$	$\eta > 0.60$	$\eta > 1.0$
	D. Load-carrying capacity loss β_h, β_v	$\beta_h > 0\%$ $\beta_v > 5\%$	$\beta_h > 2\%$ $\beta_v > 10\%$	$\beta_h > 5\%$ $\beta_v > 25\%$	$\beta_h > 20\%$ $\beta_v > 50\%$
Isolation bearing	E. Drift ratio θ	$\theta > 0.007$	$\theta > 0.015$	$\theta > 0.025$	$\theta > 0.050$
	B. Displacement δ	$\delta > 0$mm	$\delta > 50$ mm	$\delta > 100$ mm	$\delta > 150$ mm
	F. Shear strain γ	$\gamma > 100\%$	$\gamma > 150\%$	$\gamma > 200\%$	$\gamma > 250\%$

A. Choi et al. (2004); B. Hwang et al. (2001); C. Karim and Yamazaki (2007); D. Mackie and Stojadinović (2004); E. Yi et al. (2007); F. Zhang and Huo (2009)

the shear strain γ is selected as the damage index (DI) for isolation bearings under different limit states (LS).

3.2 Convex model method

The detailed calculation method consists of the following steps:

1. Choose uncertain parameters of isolated bridge. The standard random variable δ is sampled by the LHS method and is satisfied with the necessary condition $\delta_1^2 + \delta_2^2 \leq 1$. Sampling results should be transformed into structure parameters and then nonlinear time history analysis would be carried out. Moreover, the number of standard variables must guarantee the enough accuracy of response surface.
2. Conduct the nonlinear time history analysis of the structure using OpenSees. The structural seismic responses, i.e. shearing strain of LRBs and curvature of piers, can be obtained under different peak ground accelerations (PGAs).
3. Fit the seismic fragility response surface of the isolated continuous bridge. The quadratic polynomial is selected to fit the response surface of seismic fragility based on to least square method. The selected samples are treated as the training set with quadratic polynomial response surface method to calculate the limit state function. Furthermore, reasonable selection of experimental points and iterative calculation can ensure that polynomial functions are converged to real limit state function as far as possible.

   The fitting function $\overline{S}(\boldsymbol{\delta}, I = i)$ of output variables can be written as follows

$$\overline{S}(\boldsymbol{\delta}, I = i) = a + \sum_{i=1}^{n} b_i \delta_i + \sum_{i=1}^{n} \sum_{j=1}^{n} c_{ij} \delta_i \delta_j \tag{9}$$

   where n is the number of random variables, a is the constant term, b_{i} ($i = 1,\ldots,\mathrm{n}$) are linear coefficients, c_{ij}($i = 1,\ldots,\mathrm{n}$; $j = 1,\ldots,\mathrm{n}$) are quadratic coefficients and δ_i, δ_j are uncertain variables.

   Regression coefficients in response surface functions can be obtained by the least square estimation, and the number of undetermined coefficients is (n + 1)(n + 2)/2. And the real responses of structure can be approximated by response surface functions in subsequent analysis after response surface functions of the structure are obtained.
4. Substitute Eq. (9) into Eq. (5) to replace $S(\boldsymbol{\delta}, I = i)$. Using function 'fmincon' in MATLAB to solve constrained optimization problems with constraint conditions $\delta_1^2 + \delta_2^2 \leq 1$ and $|\delta_3| \leq 1$, $S_{\max}(I = i)$ and $S_{\min}(I = i)$ can be calculated by iteration. The function command 'fmincon' can be adopted.

$$[x,\ \mathrm{fval},\ \mathrm{exitflag}] = \mathrm{fmincon}(\text{'bearings'},\ [0,\ 0,\ 0.5],\ [],\ [],\ [],\ [],\ 1,\ u,\ \text{'constrains'});$$

   where, x returns regression coefficients, fval returns minimum values of the function, exitflag returns states of output values, [0, 0, 0.5] is the initial iteration value. Number 1 and u represent the lower and upper limit of parameters, respectively. The 'constrains' is defined as the nonlinear constraint function which must meet $\delta_1^2 + \delta_2^2 \leq 1$.
5. Acquire the values of $S_{\max}$ and $S_{\min}$when the structure is subjected to the ith earthquake excitation at a given PGA from step 1) to 4). Due to the random of earthquake excitation, $S_{\max}$ and $S_{\min}$ are two uncertain variables. Thus, the

corresponding maximum and minimum seismic responses of the structure at different PGAs can be obtained.

6. Combined with damage indices as described before, seismic fragility curves of different damage states of LRBs and piers can be derived by Eq. 10. Thus, the maximum and minimum failure probability can be solved according to Eq. 11.

$$P_f = \frac{n\{S \geq LS|IM|\}}{N} \tag{10}$$

where n is the number of earthquake ground motions which satisfies failure conditions, and N is the total number of earthquake ground motion records.

$$\begin{aligned} &P_{f,\min}(im) = P(S_{\min} \geq LS|IM), P_{f,\max}(im) = P(S_{\max} \geq LS|IM) \\ &P_{f,\min}(im) \leq P_f(im) \leq P_{f,\max}(im) \end{aligned} \tag{11}$$

where $P_{f,\min}$ and $P_{f,\max}$ are the lower and upper bound of P_f, respectively.

7. Fit the failure probability P_f based on the lognormal distribution function by the command 'nlinfit' in MATLAB. Finally, the robust seismic fragility curves of LRBs and bridge piers can be obtained.

3.3 Seismic fragility of the bridge system

For bridge structures, the fragility of system is more convincing than the fragility of components (Choi et al. 2004; Nielson and DesRoches 2007; Zhang and Huo 2009). However, the fragility curve of bridge system can be constructed according to the fragility curves of bridge components (bridge piers and isolation bearings). There are two methods to deal with the complicated calculation problem. One method is using the joint probabilistic seismic demand model and capacity model of the bridge components (Nielson and DesRoches 2007), and the other method is employing the first order reliability theory to obtain the upper and lower bounds on the system fragility function. Nevertheless, the latter has been widely utilized to derive the fragility curve of the bridge system in the current study.

The common system may be divided into series, parallel and hybrid system. Because the damage states of bridge components reflect the degree of the function loss in the system, it is suitable that the bridge system is considered as a series system. For the series system, the first order bound of system can be defined as Eq. (12) using the first order reliability theory.

$$\max[P(E_i)] \leq P_{fs} \leq \min\left[\sum_{i=1}^{n} P(E_i), 1\right] \tag{12}$$

where $P(E_i)$ and P_{fs} is the failure probability of bridge components and system, respectively. The lower bound of system fragility indicates the un-conservative estimate of the failure probability of the system, whereas the upper bound gives the conservative estimate of the failure probability of the system.

When the failure events of components are independent each other in the statistical sense, the upper bound can be expressed as follows

$$P_{fs} \leq 1 - \prod_{i=1}^{n} [1 - P(E_i)] \tag{13}$$

3.4 Probabilistic seismic performance evaluation of the bridge

The next-generation performance-based seismic design evaluation method, which is based on the full probability theory, had been proposed by PEER. The propose of probabilistic seismic demand analysis of structures is to predict the annual average exceeding frequency (λ_{EDP}) of engineering demand parameters (EDP). In this paper, the curvature of bridge piers and shear displacement of LRBs are assigned as the EDP.

$$\lambda(EDP > edp) = \int P(EDP > edp|IM = im)\left|\frac{d\lambda(im)}{d(im)}\right|dim \tag{14}$$

where IM is the intensity measure of earthquake ground motion(e.g. PGA. Sa(T1)). $P(EDP > edp|IM = im)$ is the conditional probability of reaching a certain limit state (LS) under different IM, which is also known as the seismic fragility analysis of structures, $\lambda(im)$ is the annual average exceeding frequency related to IM.

According to the energy law (Sewll et al. 1996), $\lambda(im)$ can be expressed as

$$\lambda(im) = k_0 im^{-k} \tag{15}$$

where k_0 and k can be calculated by fitting method according to PGA under the two seismic fortification criterion and characteristic of the bridge site. $P(EDP > edp|IM = im)$ is generally assumed as the lognormal distribution, which can be expressed as follows

$$P(EDP > edp|IM = im) = 1 - \Phi\left(\frac{\ln(im) - \ln(\eta_{edp})}{\beta_{edp}}\right) \tag{16}$$

Where η_{edp} and β_{edp} can be obtained by the least square nonlinear fitting of the seismic fragility curves under the different PGA.

The annual average exceeding frequency (λ_{EDP}) can be rewritten by substituting Eqs. (16) and (15) into Eq. (14)

$$\lambda(EDP > edp) = k_0 \eta_{edp}^{-k} \exp\left(\frac{1}{2}k^2\beta_{edp}\right) \tag{17}$$

The probability of earthquake occurrence is assumed as the Poisson distribution model, seismic hazard exceeding probability (EDP > edp) of the bridge in 50 years can be expressed as

$$P_{50}(EDP > edp) = 1 - e^{-\lambda(EDP > edp)\times 50} \tag{18}$$

4 Seismic fragility analysis of isolated continuous girder bridge

4.1 Structural properties and analytical modeling of the bridge

The bridge was built in Tibet located in the southwest of China in 2003, which is a reinforced concrete isolated continuous bridge with five equal spans and an overall length of 100 meters. The geometric detail of the seismic isolated continuous girder bridge is presented in Fig. 1, respectively. The seismic isolation bearing is used to connect the girder and the tops of the bridge piers. The expansion joints in this bridge are set on the proscenia

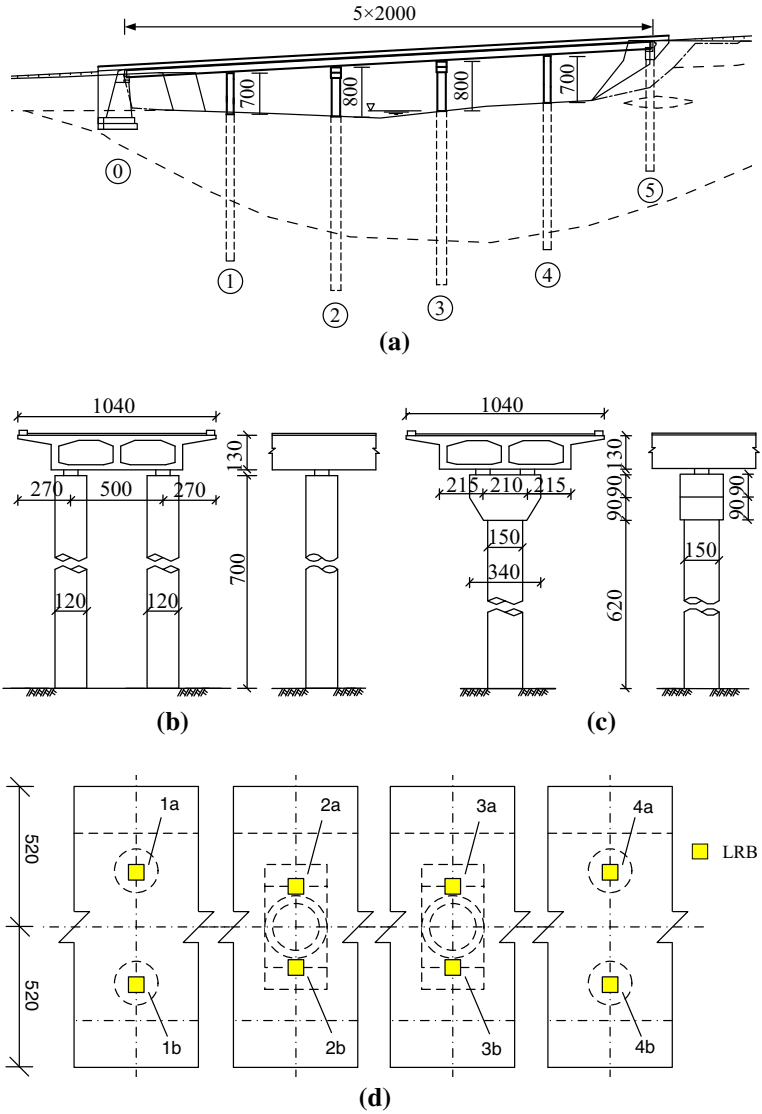

Fig. 1 Geometric details of the seismic isolated continuous girder bridge. **a** Longitudinal view of the bridge. **b** Double column bridge pier. **c** Single column bridge pier. **d** Arrangement chart of LRBs on the top of bridge piers

of both sides and the girder is supported by a gravity U-shaped abutment with an expansion base at each end of the bridge. The material parameters used in the bridge are shown in Table 2. The seismic fortification intensity of this site is 9; the site classification type is II, and the characteristic period of site is 0.4 s. The corresponding fortification peak acceleration of earthquake ground motion is 0.40 g in the horizontal direction of the bridge.

Using the finite element analysis software OpenSees, the box section girder is modeled with an elastic beam-column element, while a nonlinear beam-column element is adopted in the finite element modeling of bridge piers. A constitutive model of concrete is selected,

Table 2 Geometries and material properties of the bridge

Properties	Bridge piers	Girder
Concrete type	C30	C40
Elastic modulus of concrete (MPa)	3.00×10^4	3.25×10^4
Compressive strength standard values of concrete ($N/mm^{2)}$	20.1	26.8
Tensile strength standard values of concrete ($N/mm^{2)}$	2.01	2.39
Longitudinal rebar in bridge piers	Pier1, Pier4 HRB335 28Φ25	–
	Pier2, Pier3 HRB335 40Φ25	
Lateral rebar in bridge piers	HPB300 Φ10@100	–
Thickness of concrete cover (mm)	Pier1, Pier4 70	–
	Pier2, Pier3 80	

which represents experimental results for the confined concrete and non-confined concrete in a circular cross-section subjected to the axial force (Fig. 2). The elastic-linear hardening (bilinear) model is used for the rebar (Fig. 3). Both models are represented with uniaxial materials in OpenSees.

In Fig. 3, f_y is the yield strength of the rebar. E_s is the elastic modulus, E_0 is the secondary hardening stiffness, and $E_0 = 0.01E_s$. The mechanical properties of compression rebar are considered to be the same as those of tensile rebar in this case.

The non-linear material properties of bridge (Fig. 4) piers are considered and the cross section of the bridge pier is divided into some elements to form the concrete and rebar fiber based on the element types described above and the constitutive model of the materials (Fig. 5).

The force–displacement relationship of the LRB500 type isolation bearing is shown in Fig. 6. The area enclosed by the hysteresis curve indicates its energy dissipating capacity. Thus, the larger this area is, the greater the equivalent damping of bearing and the stronger the energy-dissipating capacity are. The isolation bearing is usually simulated with a bi-linear model in numerical calculation, and its mechanical properties are described using the pre-yield stiffness K_1, post-yield stiffness K_2 and yield shear force Q The values of these variables are shown in Table 3.

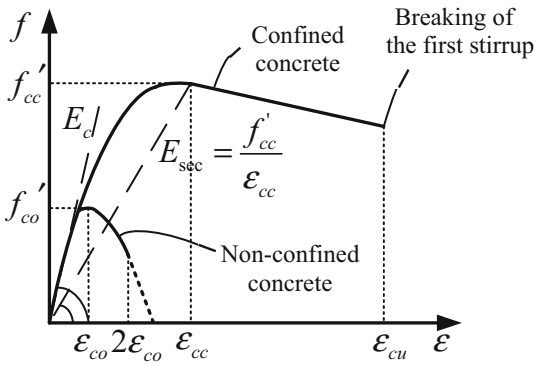

Fig. 2 Constitutive model of concrete

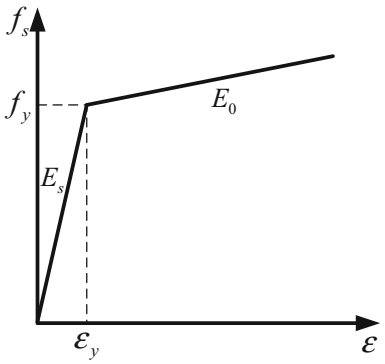

Fig. 3 Constitutive model of rebar

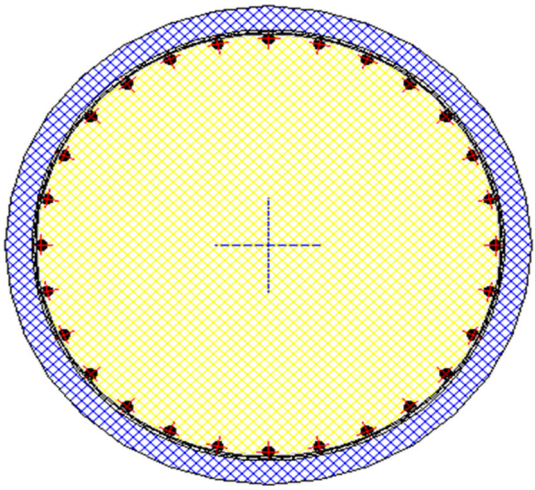

Fig. 4 Cross section of bridge pier

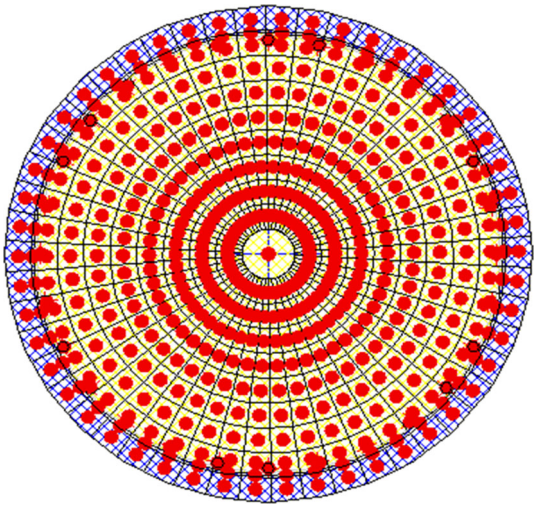

Fig. 5 Fiber cross section of pier

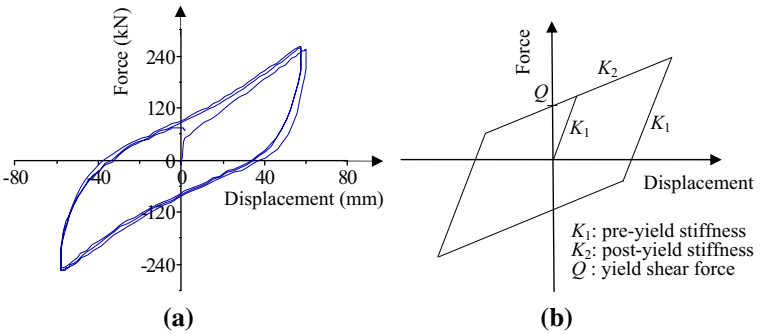

Fig. 6 Hysteresis curve and bilinear model of LRB. **a** Experiment hysteresis curve of LRB. **b** Theoretical bilinear model of LRB

Table 3 Design parameters of LRB500

Pre-yield stiffness K_1 (kN/m)	Post-yield stiffness K_2 (kN/m)	Yield shear Q (kN)	Total thickness of rubber layer t_r (mm)	Bearing height H (mm)
14,440	1413	65.2	75	150

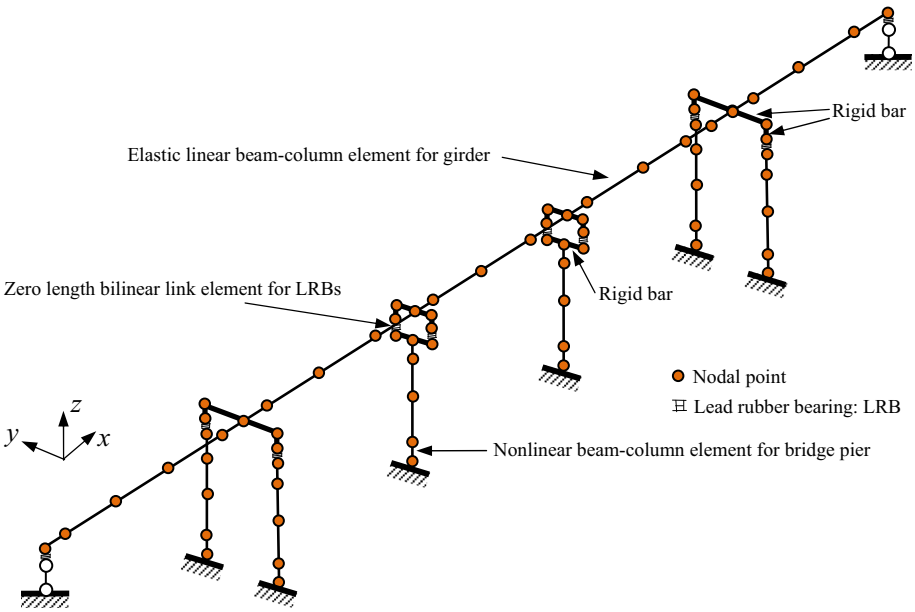

Fig. 7 3-D Finite element model of the seismic isolated continuous girder bridge in OpeeSess

The Isolation bearing is simulated by combining a zero-length element with a uniaxial material model in OpenSees. $K_2 = 0.1K_1$ when defining the parameters of the material models. A rigid bar is used to connect the isolation bearings, girder and bridge piers, and is simulated with an elastic beam-column element with a stiffness set to infinity.

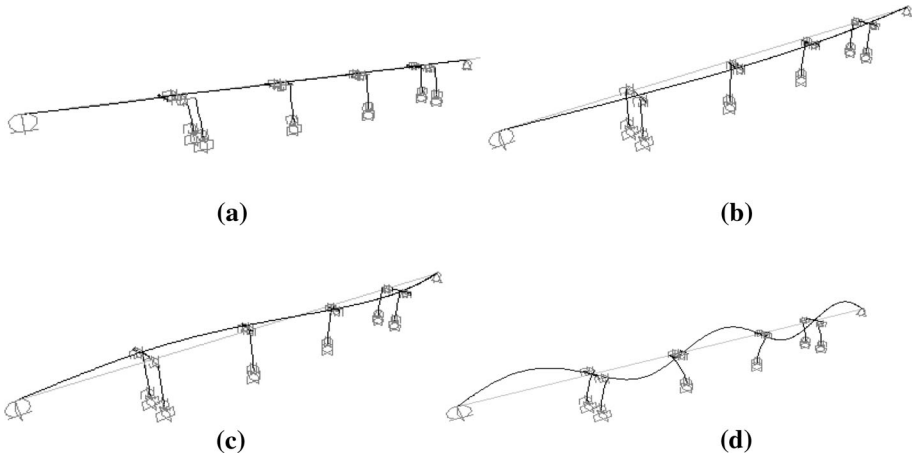

Fig. 8 The first four order mode shapes of the finite element model (SAP2000). **a** The first mode shape ($T_1 = 1.700$ s). **b** The second mode shape ($T_2 = 0.610$ s). **c** The third mode shape ($T_3 = 0.172$ s). **d** The fourth mode shape ($T_4 = 0.152$ s)

Table 4 Comparison of the first four order mode shapes of the bridge

Modal number	Period(s) (OpenSees)	Period(s) (SAP2000)	Description of mode shape
1	1.679	1.700	Longitudinal translation of girder
2	0.596	0.610	Transverse symmetric bending of girder
3	0.173	0.172	Transverse anti-symmetric bending of girder
4	0.154	0.152	Vertical bending of girder

The 3-D finite element model of the bridge by OpenSees is shown in Fig. 7. Modal analysis is conducted using the Ritz vector method on the model to obtain the dynamic characteristics of structures.

In order to verify the reliability and effectiveness of the finite element model by software package OpenSees (Fig. 7), another finite element model is also built by software package SAP2000. The modal analysis is carried out using SAP2000, and the first four order periods and mode shapes are shown in Fig. 8.

The modal analysis results using SAP2000 and OpenSees are compared in Table 4, respectively. The maximum relative deviation is 2.35% for the third order period, and the first four order mode shapes are same. It is indicated that the modal analysis of the isolated continuous girder bridge is reliable using OpenSees.

4.2 Selection of earthquake ground motions

It is important to properly select the input of the earthquake ground motion to conduct structural seismic fragility analysis, because the seismic response of structures is subsequently dependent on the uncertainty characteristics of earthquake ground motions. Characteristics of earthquake ground motions considering site type, intensity and frequency contents have a great effect on nonlinear time history response of structural

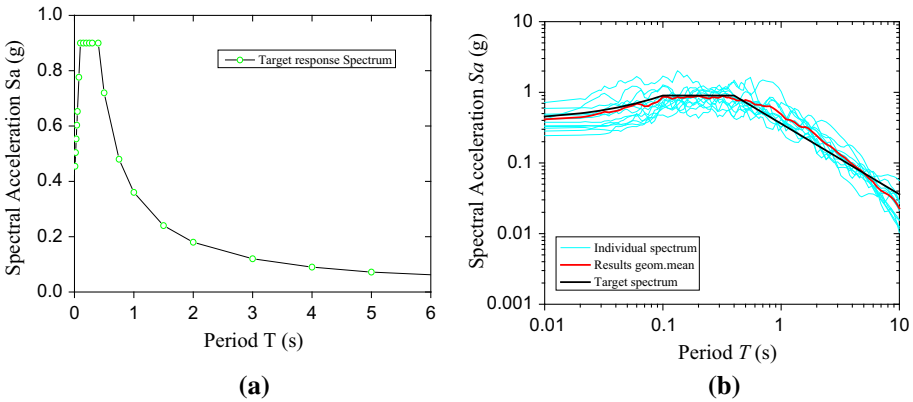

Fig. 9 Earthquake ground motion records. **a** Target response spectrum, **b** Response acceleration spectra

members. Some indices of earthquake ground motion, e.g., peak ground acceleration(PGA), peak ground velocity(PGV), peak ground displacement(PGD), spectral acceleration(Sa), spectral velocity(Sv), spectral displacement(Sd) and time duration of strong motion(Td) can be taken into account. The index PGA is a widely used to describe the severity of the earthquake ground motion (Mackie and Stojadinović 2004; Padgeet and DesRoches 2008).

The Chinese Code"Guideline for Seismic Design of Highway Bridges (JTG/T B02-01-2008 2008)" involves a demand: calculation results of the linear time history analysis should be not less than 80% that of response spectrum method under the earthquake action E1. In order to decrease the dispersion of structural response caused by different inputs of earthquake ground motion records in the time history analysis, geometry mean response spectra of the selected earthquake ground motion records should be closer to the target response spectrum(Code response spectrum). The statistical analysis of numerous ground motion records indicates that it is difficult to match well each other along the whole frequencies range of the target response spectrum. Because the first mode shape of seismic isolated bridge largely makes contribution to the structural seismic response, the selected earthquake ground motion records may be limited at a nearby range around the fundamental period of the bridge (e.g. $[T_1 - \Delta T_1, T_1 + \Delta T_2]$).

When considering the uncertainty of earthquake ground motion, the earthquake ground motion records can be obtained from the latest earthquake database disseminated by the Pacific Earthquake Engineering Research Center (PEER) in the United States according to the following steps. (1) Establish a target response spectrum, as shown in Fig. 8, according to some important information, such as the site type of this region, the seismic fortification intensity, the characteristic period, etc. (2) Select earthquake ground motion records and make their geometry mean response spectra closer to the target spectrum in the specified period range of time (e.g., $[0.1\ \text{s}, T_g]$ and $[T_1 - \Delta T_1, T_1 + \Delta T_2]$), as shown in Fig. 9. A suite of 40 selected earthquake ground motion records from the PEER database are presented in Table 5. The PGA values ranging from 0.125 to 1.126 g have been considered in the current study.

4.3 Response surface fitting of LRBs and bridge piers

According to the current studies, the yield force of LRBs δ_1, the post-yield stiffness of LRBs δ_2 and the yield strength of steel barsδ_3 are selected as uncertain variables by the

Table 5 Characteristics of the earthquake ground motion records

No.	Earthquake	Year	Station	Magnitude	Fault type	PGA(g)
77-FP	San Fernando	1971	Pacoima Dam	6.61	RV	0.171
77-FN	San Fernando	1971	Pacoima Dam	6.61	RV	0.125
126-FP	Gazli, USSR	1976	Karakyr	6.80	RV	1.123
126-FN	Gazli, USSR	1976	Karakyr	6.80	RV	1.226
139-FP	Tabas, Iran	1978	Dayhook	7.35	RV	0.573
143-FP	Tabas, Iran	1978	Tabas	7.35	RV	0.715
143-FN	Tabas, Iran	1978	Tabas	7.35	RV	0.328
162-FP	Imperial Valley-06	1979	Calexico Fire Station	6.53	SS	0.836
162-FN	Imperial Valley-06	1979	Calexico Fire Station	6.53	SS	0.852
169-FP	Imperial Valley-06	1979	Delta	6.53	SS	0.149
169-FN	Imperial Valley-06	1979	Delta	6.53	SS	0.219
173-FP	Imperial Valley-06	1979	El Centro Array#10	6.53	SS	0.275
173-FN	Imperial Valley-06	1979	El Centro Array#10	6.53	SS	0.198
174-FP	Imperial Valley-06	1979	El Centro Array #11	6.53	SS	0.238
174-FN	Imperial Valley-06	1979	El Centro Array #11	6.53	SS	0.337
178-FP	Imperial Valley-06	1979	El Centro Array #3	6.53	SS	0.370
178-FN	Imperial Valley-06	1979	El Centro Array #3	6.53	SS	0.359
180-FP	Imperial Valley-06	1979	El Centro Array #5	6.53	SS	0.484
180-FN	Imperial Valley-06	1979	El Centro Array #5	6.53	SS	0.359
181-FP	Imperial Valley-06	1979	El Centro Array #6	6.53	SS	0.519
181-FN	Imperial Valley-06	1979	El Centro Array #6	6.53	SS	0.379
183-FN	Imperial Valley-06	1979	El Centro Array #8	6.53	SS	0.329
184-FP	Imperial Valley-06	1979	El Centro Differential Array	6.53	SS	0.435
184-FN	Imperial Valley-06	1979	El Centro Differential Array	6.53	SS	0.586
185-FP	Imperial Valley-06	1979	Holtville Post Office	6.53	SS	0.351
185-FN	Imperial Valley-06	1979	Holtville Post Office	6.53	SS	0.478
728-FP	Superstition Hills-02	1987	Westmorland Fire Sta	6.54	SS	0.446
728-FN	Superstition Hills-02	1987	Westmorland Fire Sta	6.54	SS	0.300
801-FP	Loma Prieta	1989	San Jose—Santa Teresa Hills	6.93	RV-OBL	0.151
801-FN	Loma Prieta	1989	San Jose—Santa Teresa Hills	6.93	RV-OBL	0.461
803-FP	Loma Prieta	1989	Saratoga—W Valley Coll.	6.93	RV-OBL	0.966
803-FN	Loma Prieta	1989	Saratoga—W Valley Coll.	6.93	RV-OBL	0.559
879-FP	Landers	1992	Lucerne	7.28	SS	0.501
879-FN	Landers	1992	Lucerne	7.28	SS	0.324
949-FP	Northridge-01	1994	ArletavNordhoff Fire Sta	6.69	RV	0.654
949-FN	Northridge-01	1994	Arleta—Nordhoff Fire Sta	6.69	RV	0.491
1044-FP	Northridge-01	1994	Newhall—Fire Sta	6.69	RV	0.569
1044-FN	Northridge-01	1994	Newhall—Fire Sta	6.69	RV	1.001
1063-FP	Northridge-01	1994	Rinaldi Receiving Sta	6.69	RV	0.825
1063-FN	Northridge-01	1994	Rinaldi Receiving Sta	6.69	RV	0.475

Table 6 Bound values of uncertain variables

Uncertain variables		Minimum value	Mean value	Maximum value	Deviation
Yield force of LRB500 Q (kN)	x_1	52.16	65.2	78.24	0.2
Post-yield stiffness of LRB500 K_2 (kN/m)	x_2	1.1304	1.413	1.6956	0.2
Yield strength of steel bar f_y (N/mm^2)	x_3	252	300	348	0.16

Table 7 Calculation values of sample points of uncertain variables

Sample point	Uncertain variables					
	x_1	Q (kN)	x_2	K_2 (kN/m)	x_3	f_y (N/mm^2)
1	0.4725	71.3614	−0.0109	1.560772	0.8768	411.0975
2	0.1237	66.81305	0.5229	1.487069	0.5604	357.664
3	−0.6316	56.96394	0.2621	1.181211	−0.3248	390.2903
4	0.1944	67.73498	−0.8202	1.176096	0.2157	406.3952
5	−0.4001	59.9827	−0.8383	1.569702	0.4825	329.5589
6	−0.7318	55.65733	0.5545	1.641991	−0.7904	332.3477
7	−0.5748	57.70461	0.8103	1.432076	−0.7442	383.252
8	0.7899	75.5003	0.0675	1.597142	0.0991	424.4137
9	−0.515	58.4844	0.6516	1.321494	0.781	413.3612
10	−0.8925	53.5618	−0.3238	1.296541	0.5979	405.5622
11	−0.1166	63.67954	−0.4121	1.507897	0.4687	413.2887
12	−0.8133	54.59457	0.3358	1.47147	0.5967	430.7518
13	−0.3853	60.17569	0.2069	1.427752	0.886	399.4474
14	−0.0879	64.05378	0.0522	1.542826	0.3674	332.8548
15	−0.7967	54.81103	0.4594	1.572047	−0.7358	330.229
16	−0.3358	60.82117	0.5628	1.293178	−0.7793	331.0922

sensitivity analysis of structures (Fan et al. 2014). Moreover, x_1 and x_2 are described with unit circle model while x_3 is described with interval model since it is not correlated with the other two variables. Detailed uncertainties are illustrated in Table 6 and 16 sample points are shown in Table 7.

Based on above mentioned sample points, 16 response sample points are treated as training set to conduct the regression analysis. For instance, when the El Centro ground motion (Imperial Valley-06, 1979, PGA = 0.4 g) is selected, the regression coefficients are listed in Table 8.

Quadratic polynomial response surface function of LRBs can be expressed as Eq. (19)

$$\begin{aligned}\bar{S}(\delta|IM = 0.4\,\mathrm{g}) = {} & 0.109376 - 0.00322\delta_1 - 0.0052\delta_2 - 0.00775\delta_3 \\ & - 0.00412\delta_1^2 - 0.00322\delta_1\delta_2 - 0.00751\delta_1\delta_3 \\ & + 0.001345\delta_2^2 + 0.00913\delta_2\delta_3 + 0.002761\delta_3^2\end{aligned} \tag{19}$$

Table 8 Regression coefficients under El Centro ground motion (PGA = 0.4 g)

Regression coefficients	a	b_1	b_2	b_3	c_{11}	c_{12}	c_{13}	c_{22}	c_{23}	c_{33}
LRBs ($\times 10^{-3}$)	109.376	−3.22	−5.2	−7.75	−4.12	−3.22	−7.51	1.345	9.13	2.761
Piers ($\times 10^{-5}$)	172.6	9.34	13.5	18.3	2.78	7.8	16.7	−4.8	−25	−8.1

Similarly, quadratic polynomial response surface function of piers can be written as Eq. (20)

$$\begin{aligned}\bar{S}(\delta|IM = 0.4\text{g}) = {} & 0.001726 + 9.34 \times 10^{-5}\delta_1 + 0.000135\delta_2 + 0.000183\delta_3 \\ & + 2.78 \times 10^{-5}\delta_1^2 + 7.8 \times 10^{-5}\delta_1\delta_2 + 0.000167\delta_1\delta_3 \\ & - 4.8\text{E} \times 10^{-5}\delta_2^2 - 0.00025\delta_2\delta_3 - 8.1 \times 10^{-5}\delta_3^2\end{aligned} \tag{20}$$

Using maximum relative deviation Q to assess and analyze the obtained response surface (Duan and Zhao 2009). And Q is the maximum ratio of sample fitting value to calculation value, Q can be defined as Eq. (21)

$$Q = \max\left\{\frac{Y_i - M_i}{Y_i}\right\}, \quad i = 1, \ldots, n \tag{21}$$

where Y_i represents observation values of response variables (i.e., calculation values), M_i represents the fitting values of response variables.

The comparisons of absolute and relative deviation of displacement of lead rubber bearings and curvature of bridge piers are presented in Table 9.

The maximum relative deviations are almost less than 5% in Table 8. Extreme values can be found by conducting optimization search in the whole random variable space after acquiring response surface function $\bar{S}$. It should be noticed that origin function values need to be negative using function 'fmincon' in MATLAB to solve maximum values, while the calculation results needs to be absolute due to function 'fmincon' means seeking for the minimum value of functions. For example, the optimization results of isolated continuous girder bridge subjected to El Centro earthquake exciation (Record number: 184-FN, PGA = 0.4 g) are shown in Table 10.

From Table 10 it can be observed that the maximum value and minimum value of response surface function contain the real response values. The response surface function value is more inclusive and safer by the optimization search.

4.4 Fragility curves of bridge piers and LRBs

As described above, each earthquake ground motion records with different PGA can be used to calculate S_{max} and S_{min}. In other words, N values of S_{max} and S_{min} will be obtained under each different PGA. Then, fragility curves of bridge components can be derived according to the frequency method. Equation (11) is used to solve the upper bound $P_{f,max}$ and lower bound $P_{f,min}$ of fragility curves of LRBs and bridge piers subjected to earthquake excitations (PGA = 0.2 g, 0.4 g, 0.8 g, 1.0 g). The fragility curves of $P_{f,max}$ and $P_{f,min}$ of LRBs and bridge piers are illustrated in Figs. 10, 11, 12, 13, respectively.

Figure 14 shows the comparison diagrams of seismic fragility curves of the LRB under four limit states, $P_{f,max}$ and $P_{f,min}$ represent the upper bound and lower bound failure

Table 9 Comparisons of absolute and relative deviation of bridge components

Displacement of LRBs	Fitting values	Absolute deviation	Relative deviation (%)	Curvature of bridge piers	Fitting values	Absolute deviation	Relative deviation (%)
0.1078700	0.10938	0.00151	1.396	0.0017537	0.00173	0.00003	1.558
0.1018160	0.09914	0.00268	2.629	0.0018773	0.00194	0.00007	−0.614
0.1054510	0.10503	0.00042	0.398	0.0018094	0.00182	0.00001	0.001
0.1157940	0.10952	0.00627	5.416	0.0015257	0.00168	0.00016	0.061
0.1144750	0.11081	0.00367	3.202	0.0015944	0.00168	0.00008	−0.010
0.1045710	0.10889	0.00432	4.133	0.0018032	0.00171	0.00009	−0.011
0.1038740	0.10787	0.00400	3.849	0.0018295	0.00171	0.00012	0.0216
0.1086590	0.10662	0.00204	1.881	0.0017062	0.00176	0.00006	0.007
0.1003230	0.10248	0.00215	2.147	0.0019091	0.00186	0.00005	0.074
0.1114540	0.11150	0.00005	0.043	0.0016350	0.00163	0.00001	0.001
0.1128470	0.10846	0.00439	3.890	0.0015852	0.00168	0.00009	−0.029
0.1056340	0.10754	0.00190	1.800	0.0018086	0.00176	0.00005	−0.011
0.1079510	0.11039	0.00244	2.258	0.0016874	0.00164	0.00005	0.015
0.1081970	0.10878	0.00058	0.540	0.0017152	0.00171	0.00000	0.002
0.1053620	0.10732	0.00196	1.856	0.0018367	0.00177	0.00007	0.126
0.1053860	0.10811	0.00273	2.588	0.0017465	0.00169	0.00005	0.011
0.1120150	0.10985	0.00217	1.935	0.0016514	0.00170	0.00005	0.009

Table 10 Real response values and optimization values of LRBs and bridge piers

Structural response	Maximum value $S_{\max}$ (m)		Minimum value $S_{\min}$ (m)	
	LRBs	Bridge piers	LRBs	Bridge piers
Real response values	0.1157940	0.1115020	0.1003230	0.0991390
Optimization values	0.1366321	0.1366321	0.0895304	0.0895304

probability, and $P_f\,(\delta = 0)$ denotes the failure probability without considering uncertainties of structure parameters, respectively. It can be observed that $P_f\,(\delta = 0)$ is located between $P_{f,max}$ and $P_{f,min}$ under the same given PGA, and uncertainty of the LRB will make a great effect on the fragility curves of the LRB.

Figure 15 shows the comparison diagrams of fragility curves of the bridge pier under four limit states. The $P_{f,min}$ fragility curves are very close to $P_f\,(\delta = 0)$ curves, whereas the $P_{f,max}$ fragility curves are much greater than $P_f\,(\delta = 0)$ curves. It is indicated that the lower bound of uncertain variables are not sensitive to the fragility curves of bridge piers.

Figure 14, 15 show that $P_{f,max}$ seismic fragility curves are totally greater than $P_{f,min}$, and the failure probability of LRB are greater than that of bridge piers, especially when PGAs range from 0.1 g to 0.4 g. Taking slight damage state of LRB as an example, as illustrated in Fig. 14, the $P_{f,max}$ fragility curve of LRB gets close to 0.8 (PGA = 0.4 g), while it starts from PGA = 0.6 g in $P_{f,min}$ fragility curve, and the fragility curve $P_f\,(\delta = 0)$ without considering uncertainties of structure parameters locates between $P_{f,max}$ and $P_{f,min}$.

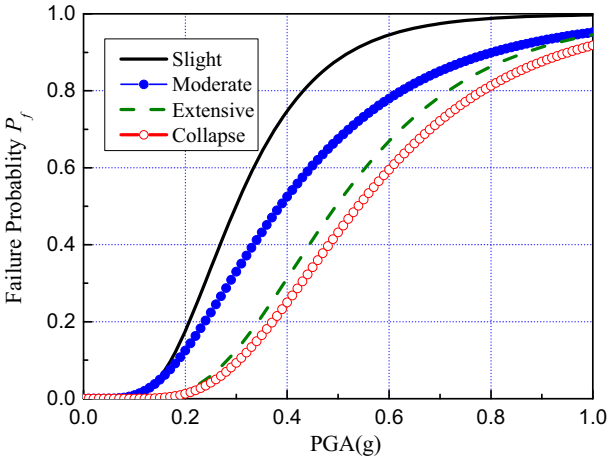

Fig. 10 $P_{f,max}$ fragility curves of LRBs

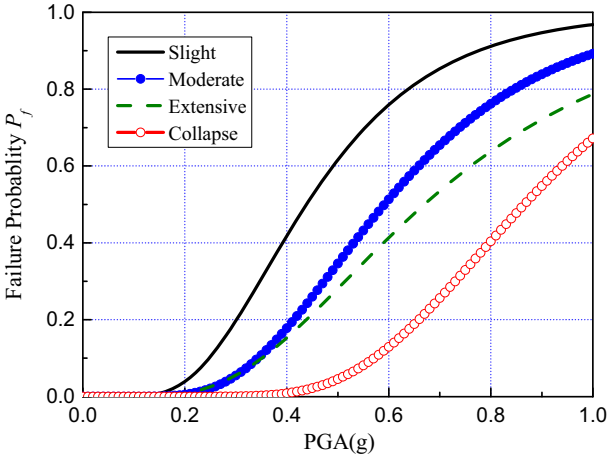

Fig. 11 $P_{f,min}$ fragility curves of LRBs

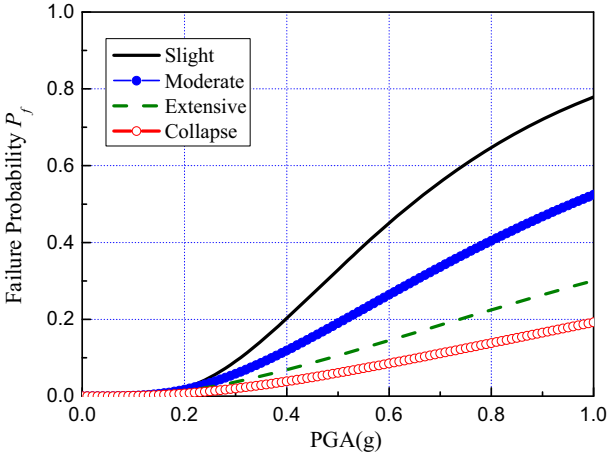

Fig. 12 $P_{f,max}$ fragility curves of bridge piers

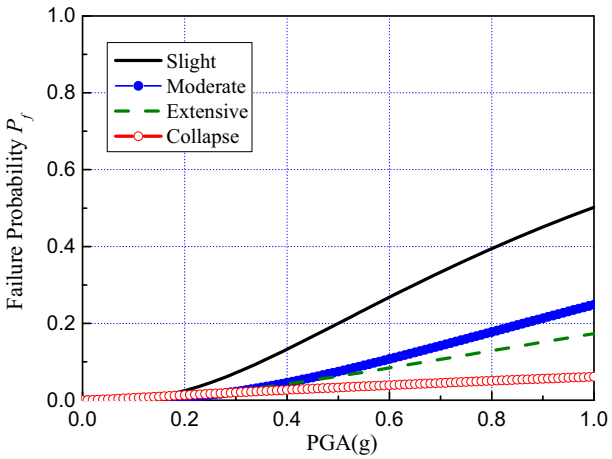

Fig. 13 $P_{f,min}$ fragility curves of bridge piers

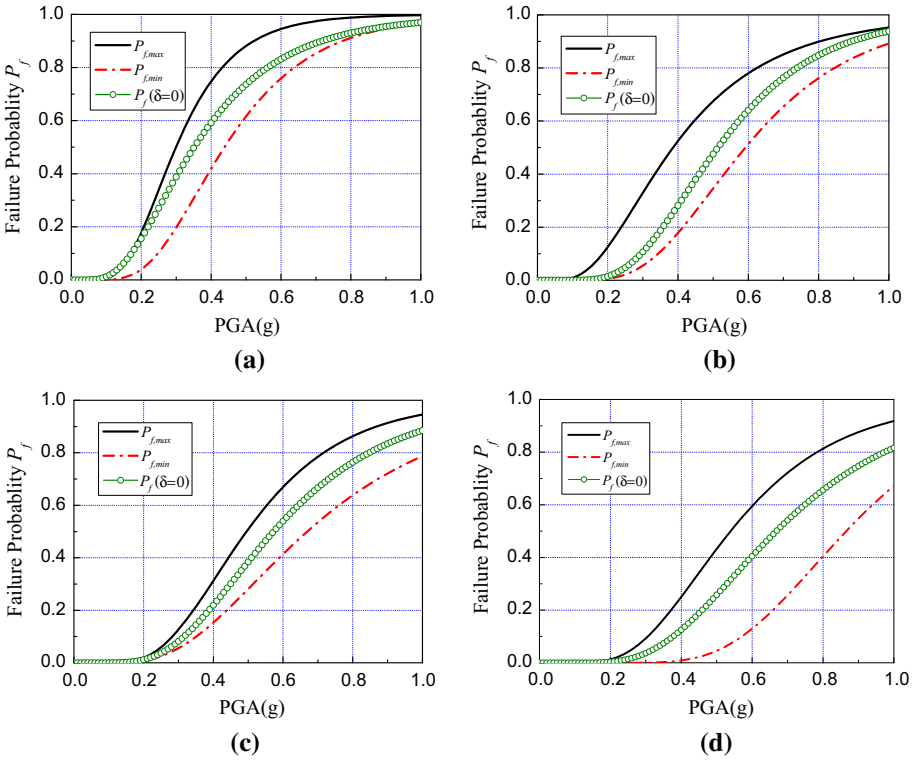

Fig. 14 $P_{f,max}$, $P_{f,min}$ and $P_f(\delta = 0)$ fragility curves of LRB. **a** Slight. **b.** Moderate. **c** Extensive. **d** Collapse

Therefore, failure probability P_f would be underestimated when uncertainties of structure parameters are ignored. In view of safety, $P_{f,max}$ fragility curves of LRB and bridge piers had better be advised to employ in designing new bridges and prioritization of retrofitting strategies of existing bridges.

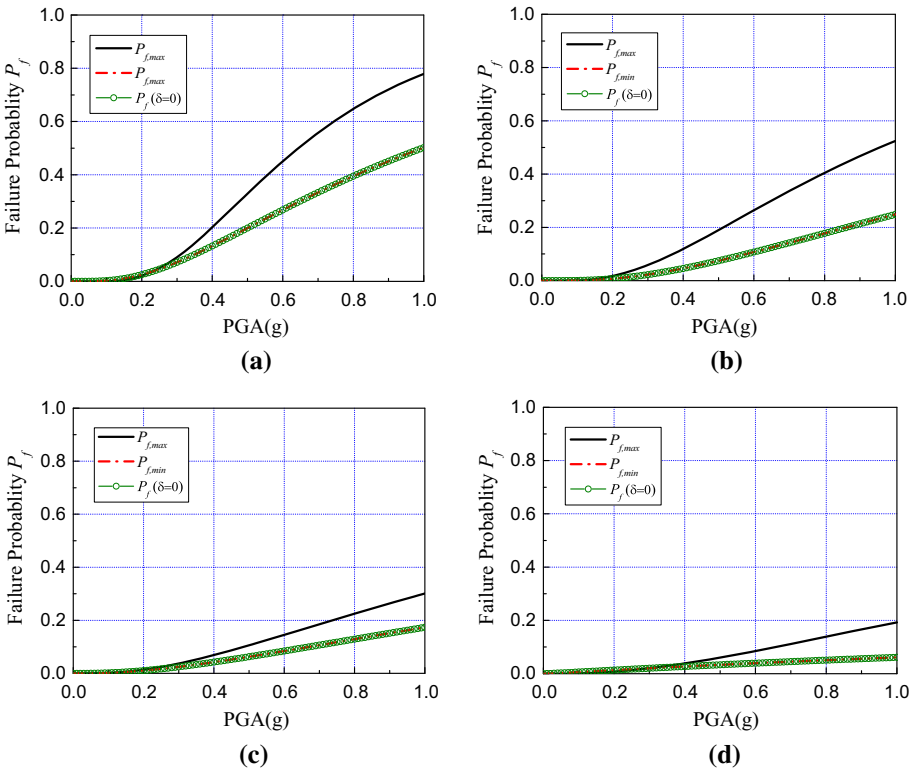

Fig. 15 $P_{f,max}$, $P_{f,min}$ and P_f ($\delta = 0$) fragility curves of bridge pier. **a** Slight. **b** Moderate. **c** Extensive. **d** Collapse

Though the probabilistic distribution functions of LRBs are rarely mentioned in the recent research, national standard for rubber bearings provides the bound values of these parameters (such as allowable deviation of shear property of bearings type S-B is within ±20% (GB/T 20688.1-2007 2007). Therefore, the uncertainty of LRB design parameters can be properly taken account into using the convex model approach, whereas that is not considered in cloud method. Figures 16 and 17 present the fragility of the lead rubber bearing(LRB) used in the bridge system under four limit states. Figure 16 displays that the failure probability $P_{f,max}$ using convex model is greater than that using cloud method for the given limit state. However, the failure probability $P_{f,min}$ using convex model is less than that using cloud method for the given limit state in Fig. 17. It is indicated that the fragility curves of LRB using cloud method is distributed between $P_{f,min}$ and $P_{f,max}$. Consequently, if the the uncertainty of LRB design parameters is not properly considered, the seismic fragility of LRB will be underestimated. The median value of PGA, which corresponds to failure probability $P_f = 50\%$, is determined for the LRB at each damage level. That comparison is presented in Table 11. From this table it can be observed that the maximum percent difference of median values of PGA is −25.00% between the cloud method and convex model-$P_{f,max}$ at the collapse level, while the minimum percent difference is 9.84% between the could method and convex model-$P_{f,min}$ at the extensive level.

In view of structural safety in designing new bridges and prioritization of retrofitting strategies of old bridges, the failure probability $P_{f,max}$ had better be served as the seismic

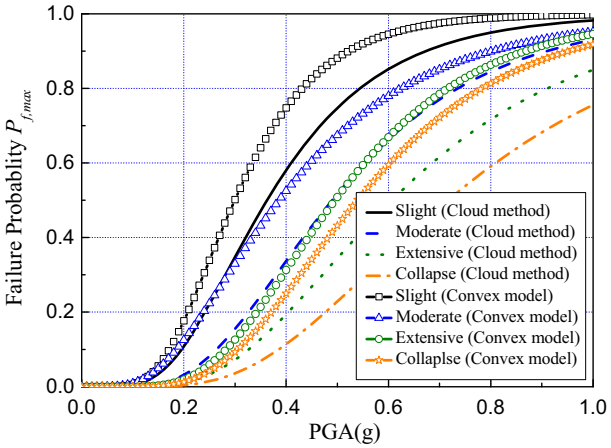

Fig. 16 $P_{f,max}$ fragility curves of LRB

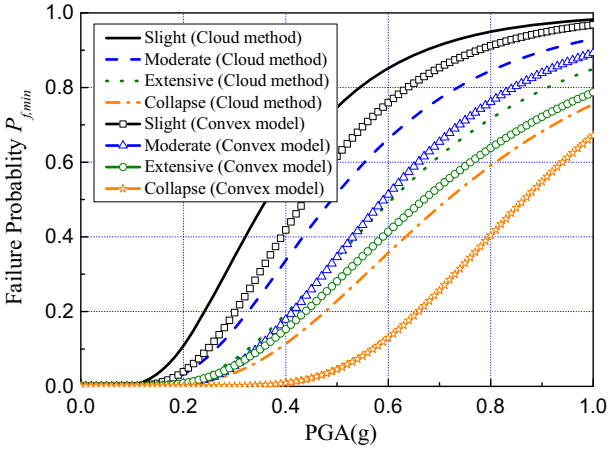

Fig. 17 $P_{f,min}$ fragility curves of LRB

fragility curves, which are referred as robust seismic fragility curves. In addition, similar trends can also be observed in the seismic fragility curves for the bridge pier in Figs. 18 and 19.

The numerical results as depicted in Figs. 16, 17, 18 and 19 illustrate the relative likelihood of reaching/exceeding certain limit state at a given PGA input for bridge components (isolation bearing and bridge pier), which indicates that the damage of LRB is prior to that of the bridge pier. Because of the energy dissipation of isolation bearings, the earthquake action of bridge piers is greatly decreased and seismic safety of bridge piers are assured.

4.5 Seismic fragility curve of bridge system

The seismic fragility curve of a bridge system can be subsequently obtained by the seismic fragility curves of bridge components (bridge piers and isolation bearings). This can be carried out by the Monte Carlo simulation, but this method is extremely time-consuming.

Table 11 Median value of PGA for LRB with respect to $P_f = 50\%$

Damage state	Slight	Moderate	Extensive	Collapse
Cloud method	0.36 g	0.49 g	0.61 g	0.72 g
Convex model-$P_{f,max}$ (percent difference)	0.31 g (−13.89%)	0.39 g (−20.41%)	0.50 g (−18.03%)	0.54 g (−25.00%)
Convex model-$P_{f,min}$ (percent difference)	0.44 g (22.22%)	0.58 g (18.37%)	0.67 g (9.84%)	0.87 g (20.83%)

The percent difference of median value of PGA is defined as the ration: (convex model—cloud method)/cloud method. Values in parentheses denote the percent difference of median valued of PGA

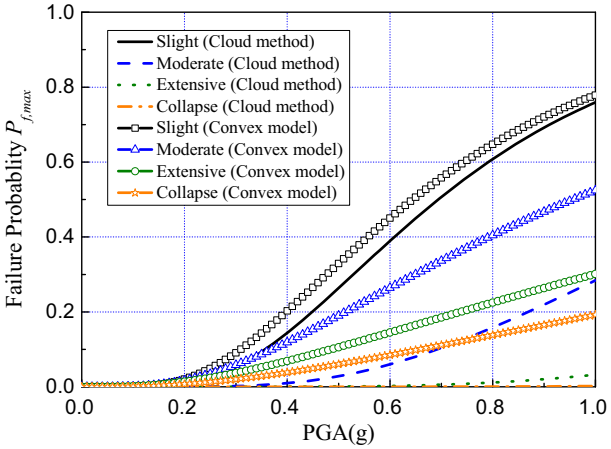

Fig. 18 $P_{f,max}$ fragility curves of bridge pier

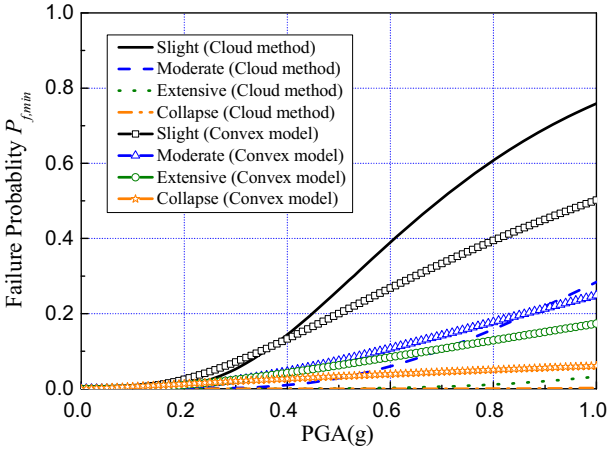

Fig. 19 $P_{f,min}$ fragility curves of bridge pier

Therefore, the first order reliability theory (Eq. 12) is adopted to construct the seismic fragility curve of bridge system. In view of the structural seismic safety, the upper bound of the fragility curve of the bridge system is assigned.

The fragility curves of the LRB and bridge pier are obtained using the convex model approach (according to the upper bound $P_{f,max}$), and then the fragility curves of the bridge system can be constructed using the first order reliability theory. Figure 20a–d present the robust seismic fragility curves of the bridge system, LRB and bridge pier under four limit states, respectively. It can be observed that the robust seismic fragility curve of the bridge system is closer to the robust seismic fragility curve of LRB at each limit state, whereas it is much greater than fragility curve of the bridge pier. The results indicate that the seismic fragility of the bridge system is largely dictated by the fragility of LRB.

4.6 Probabilistic seismic performance evaluation of the bridge system

The seismic fragility curves of the bridge system have been derived under four limit states using cloud method and convex model approach, respectively. Exceeding probability curves of bridge system in 50 years can be calculated to conduct the probabilistic seismic performance evaluation of the bridge using structural seismic risk estimate method.

According to Chinese Code: Guidelines for seismic design of highway bridge (JTG/T B02-01-2008 2008), the two seismic fortification criterion (Table 12) and two stages design are adopted for the seismic design of the isolated continuous girder. Through the calculation of the bridge, $k_0 = 2.14563$, $k = 0.0000254$.

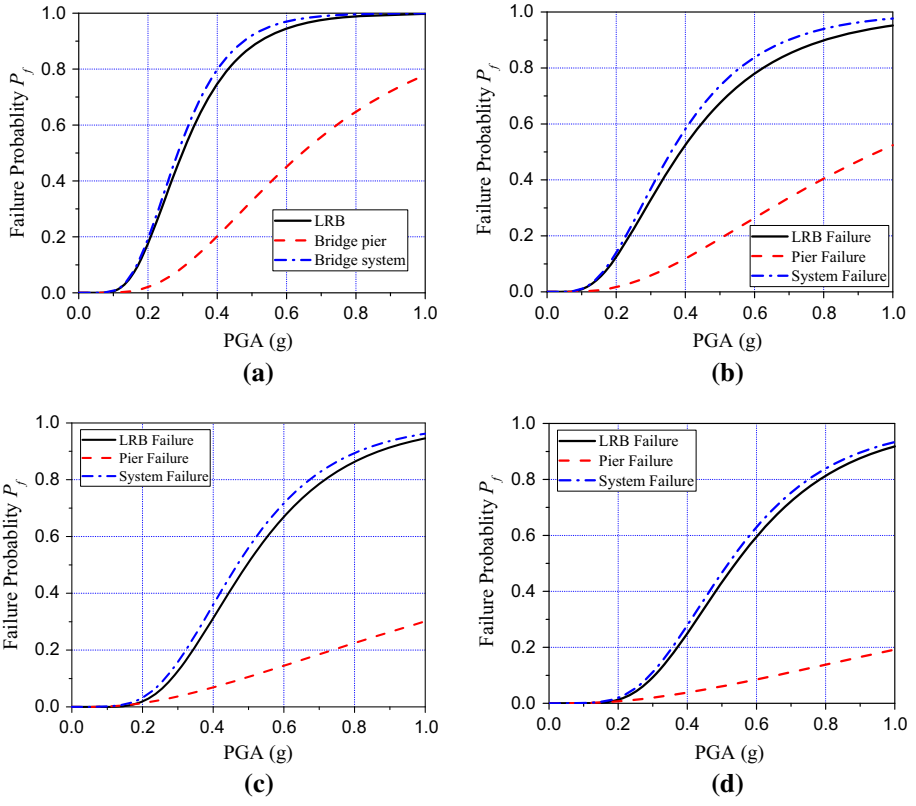

Fig. 20 Fragility curves of LRB, bridge pier and bridge system. **a** Slight. **b** Moderate. **c** Extensive. **d** Collapse

Table 12 Seismic fortification criterion of highway bridge

Performance level	Earthquake action E1	Earthquake action E2
Damage state description	Slight damage of bridge components and system will not happen, which is defined as "intact state". The recurrence interval of earthquake is 475 years	Extensive damage or collapse of bridge components and system will not happen, which is defined as "moderate state". The recurrence interval of earthquake is 2000 years
Exceeding probability in 50 years	$P_{50} = 10\%$	$P_{50} = 2.47\%$

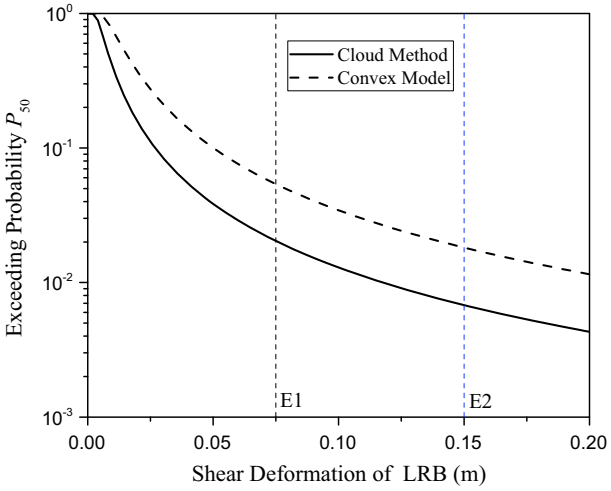

Fig. 21 Exceeding probability of LRB

Under the earthquake action E1 and E2, the exceeding probability curves of the isolation bearing and bridge pier in 50 years are calculated using the cloud method and convex model, respectively (Figs. 21, 22). it can be observed that the exceeding probability of LRB is 4.49% (convex model) and 2.05% (cloud method), while that of the bridge pier is 1.21% (convex model) and 0.86% (cloud method) when the bridge is subjected to the earthquake action E1. Under the earthquake action E2, the exceeding probability of LRB is 1.56% (convex model) and 0.67% (cloud method), while that of bridge pier is 0.39% (convex model) and 0.04% (cloud method). It is indicated that exceeding probability of bridge components using the convex model are greater than that using the cloud method. If the uncertainty of LRB design parameters can not be properly considered, the exceeding probability of isolation bearing will be underestimated. Therefore, It is suggested that calculation results based on the convex model are served as the important reference to the probabilistic seismic evaluation of bridge components in view of the structural seismic safety.

Under the earthquake action E1 and E2, the exceeding probabilities of the bridge components and bridge system in 50 years are presented in Table 13 using the convex model approach, respectively.

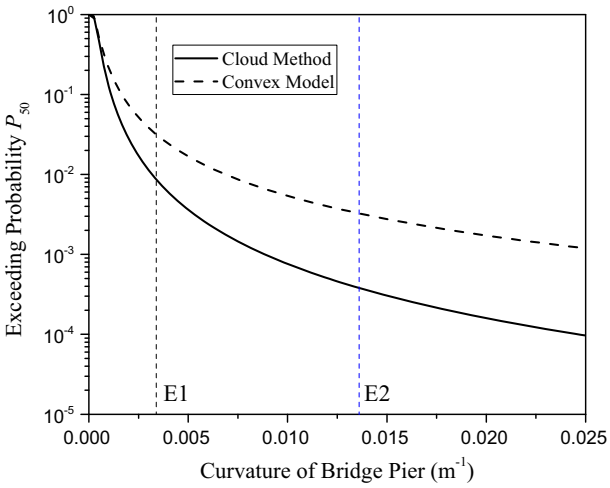

Fig. 22 Exceeding probability of bridge pier

Table 13 Exceeding probabilities of the bridge components and bridge system

Performance level	LRB	Bridge pier	Bridge system
E1 ($P_{50} = 10\%$)	$P_{50}(\delta > 0.075m) = 4.49\%$	$P_{50}(\varphi > 0.0034) = 1.21\%$	$P_{50}(\delta > 0.075m \cup \varphi > 0.0034) = 5.65\%$
E2 ($P_{50} = 2.47\%$)	$P_{50}(\delta > 0.150m) = 1.56\%$	$P_{50}(\varphi > 0.0136) = 0.39\%$	$P_{50}(\delta > 0.150m \cup \varphi > 0.0136) = 1.94\%$

δ and ϕ denote the shear deformation of LRB and curvature of bridge pier, respectively

From Table 12 it can be observed that seismic performance of the isolated continuous girder bridge fully meets the demand of two seismic fortification criterion (JTG/T B02-01-2008 2008). The exceeding probability of the bridge system is 5.65% when the bridge is subjected to the earthquake action E1. It is shown that the bridge system possess more seismic safety capacity. However, The exceeding probability of the bridge system is 1.94% under the earthquake action E2, and that is closer to 2.47%. Thus, seismic safety capacity of the bridge system is less. In addition, the exceeding probability of LRB is greater than that of the bridge pier under the same seismic fortification criterion. It is indicated that the damage of LRB is prior to that of bridge piers. The earthquake action of the bridge pier is greatly decreased through the energy dissipation of LRB. Finally, the bridge piers is preserved.

5 Conclusion

The seismic fragility curves of a five-span isolated continuous girder bridge with lead rubber bearings are derived using convex model approach and cloud method, respectively. The uncertainty of structure parameters is taken into account. The fragility curves of the bridge components and the bridge system can be potentially used to evaluate the probabilistic seismic performance of the bridge, retrofitting prioritization and post-earthquake rehabilitation decision making. The concluding remarks are summarized as follows:

- There are only a few studies on the probability distribution function of mechanical parameters of rubber bearings. However, national standard for rubber bearings (GB/T 20688.1-2007 2007) provides the bound values of design parameters. Convex model approach can be successfully introduced into the seismic fragility analysis of isolated bridges, and it is feasible and reliable for no need to assume the probability distribution of rubber bearing parameters.
- The numerical results indicate that the failure probabilities P_f of the bridge components and the bridge system using cloud method are distributed between $P_{f,min}$ and $P_{f,max}$. If the the uncertainty of structural parameters is not properly considered, the seismic fragility of the bridge components and the bridge system will be underestimated. In view of structural safety in designing new bridges and prioritization of retrofitting strategies of old bridges, the failure probability $P_{f,max}$ obtained from the convex model approach had better be served as the seismic fragility curves.
- Through the comparisons of the relative likelihood of reaching/exceeding certain limit state at a given PGA input for the bridge components, the damage of LRB is prior to that of the bridge pier. Because of the energy dissipation of isolation bearings, the earthquake action of bridge piers is greatly decreased and seismic safety of bridge piers are assured.
- The convex model-based robust seismic fragility curves of the bridge can be potentially used to the probabilistic seismic performance. The calculation results show that seismic performance of the isolated continuous girder bridge fully meets the demand of two seismic fortification criterion in 50 years. (Chinese Code: JTG/T B02-01-2008).

In summary, convex model approach can provide a new way to derive robust fragility curves of isolated bridges when double uncertainties of structural parameters and earthquake ground motions are taken into account. Future study should include the effect of abutments and the foundation on the seismic fragility analysis.

Acknowledgements The authors would like to extend their thanks to the joint financial support by National Natural Science Fund of China (51278213, 51378234) and the Innovation Foundation of the Fundamental Research Funds for the Central Universities (HUST: 2016YXMS093). The authors also gratefully acknowledge the work from reviewers.

References

Alam MS, Bhuiyan MAR, Billah AHMM (2012) Seismic fragility assessment of SMA-bar restrained multispan continuous highway bridge isolated by different laminated rubber bearings in medium to strong seismic risk zones. Bull Earthq Eng 10(6):1885–1909

Billah AHMM, Alam MS (2015) Seismic fragility assessment of highway bridges: a state-of-the-art review. Struct Infrastruct Eng 11:804–832

Choi E, DesRoches R, Nielson B (2004) Seismic fragility of typical bridges in moderate seismic zones. Eng Struct 26:187–199

Cornell CA, Krawinkler H (2000) Progress and challenges in seismic performance assessment. PEER Center News 3:1–4

Duan W, Zhao F (2009) Comparative study on response surface methods for structural reliability analysis. Chin J Constr Mach 7(4):392–397

Elishakoff I (1995) Essay on uncertainties in elastic and viscoelastic structures: from A. M. Freudenthal's criticisms to modern convex modeling. Comput Struct 56:871–895

Fan J, Long XH, Zhao J (2014) Calculation on robust fragility curves of base-isolated structure under near-fault earthquake considering base pounding. Eng Mech 31:166–172

FEMA (2006) Next-generation performance-based seismic design guidelines-program plan for new and existing buildings. Redwood City, California

GB/T 20688.1-2007(2007) Rubber bearings-part: seismic-protection isolators test methods. China Standard Press, Beijing, China
Hwang H, Liu JB, Chiu YH (2001) Seismic fragility analysis of highway bridges. Mid-America Earthquake Center Technical Report, MAEC-RR-4 Project
JTG/T B02-01-2008 (2008) Guidelines for seismic design of highway bridge. China Communication Press, Beijing, China
Karim KR, Yamazaki F (2001a) Effects of earthquake ground motions on fragility curves of highway bridge piers based on numerical simulation. Earthq Eng Struct Dyn 30:1839–1856
Karim KR, Yamazaki F (2001b) Effect of earthquake ground motions on fragility curves of highway bridge piers based on numerical simulation. Earthq Eng Struct Dyn 30:1839–1856
Karim KR, Yamazaki F (2007) Effect of isolation on fragility curves of highway bridges based on simplified approach. Soil Dyn Earthq Eng 27:414–426
Mackie KR, Stojadinovi¢ B (2004) Fragility curves for reinforced concrete highway overpass bridges. In: Proceedings of 13th World Conference on Earthquake Engineering. Paper No. 1553
McKenna F, Fenves GL (2001) The OpenSees command language manual, Version 1.2. Pacific Earthquake Engineering Research Center, University of California at Berkeley, Berkeley. http://opensees.berkeley.edu/. Accessed 10 July 2013
Moschonas IF, Kappos AJ et al (2009) Seismic fragility curves for greek bridges: methodology and case studies. Bull Earthq Eng 7:439–468
Nielson BG, DesRoches R (2007) Seismic fragility curves for typical highway bridge classes in the central and southeastern United States. Earthq Spectra 23:615–633
Padgeet JE, DesRoches R (2008) Methodology for the development of analytical fragility curves for retrofitted bridges. Earthq Eng Struct Dyn 37:157–174
Padgett JE, Nielson BG, Desroches R (2008) Selection of optimal intensity measures in probabilistic seismic demand models of highway bridge portfolios. Earthq Eng Struct Dyn 37:711–725
Pantelides CP, Tzan S (1996) Convex model for seismic design of structures-I: analysis. Earthq Eng Struct Dyn 25:927–944
Qiu Z, Wang J (2010) The interval estimation of reliability for probabilistic and non-probabilistic hybrid structural system. Eng Fail Anal 17:1142–1154
Sewell RT, Toro GR, McGuire RK (1996) Impact of ground motion characterization on conservatism and variability in seismic risk estimates. Rockville, MD, USA: US, Nuclear Regulatory Commission, Report NUREG/CR-6467
Shinozuka M, Feng MQ, Lee J et al (2000a) Statistical analysis of fragility curves. J Eng Mech 126:1224–1231
Shinozuka M, Feng MQ, Kim H et al (2000b) Nonlinear static procedure for fragility curve development. J Eng Mech 126:1287–1295
Shome N (1999) Probabilistic seismic demand analysis of nonlinear structures. Ph.D. Dissertation, Stanford University
Yi JH, Kim SH, Kushiyama S (2007) PDF interpolation technique for seismic fragility analysis of bridges. Eng Struct 29:1312–1322
Zhang J, Huo YL (2009) Evaluating effectiveness and optimum design of isolation devices for highway bridges using the fragility function method. Eng Struct 31:1648–1660